Astronomy
&
Astrophysics

Abundances in planetary nebulae: Hb 5[*]

S. R. Pottasch[1] and R. Surendiranath[2]

[1] Kapteyn Astronomical Institute, PO Box 800, NL 9700 AV Groningen, The Netherlands
    e-mail: pottasch@astro.rug.nl
[2] Indian Institute of Astrophysics, Koramangala II Block, Bangalore-560034, India

ABSTRACT

The ISO spectra of the bilobal planetary nebula Hb 5 are presented. These spectra are combined with the spectra in the visual wavelength region to obtain a complete, extinction corrected, spectrum. The chemical composition of the nebula is then calculated in several ways. First by directly calculating and adding individual ion abundances, assuming that all the ionic lines are formed in an ionized region surrounding the ionizing star. Secondly by building an "end-to-end model" nebula in which we have included a neutral region and a photodissociation region (PDR) beyond the ionized nebula. In this way we attempt to interpret the molecular hydrogen lines observed by ISO in a more self-consistent way. In the final analysis, the model is found to be basically heuristic, but gives new insights about the PDR and the PN. The implications of these are discussed.

Key words. ISM: abundances – planetary nebulae: individual: Hb 5 – stars: evolution – HII regions

1. Introduction

Hb 5 (Hubble 5) is a rather large bipolar nebula. An HST image in visible light is shown as Fig. 1. In many ways the morphology is similar to that of NGC 6537. Most of its emission is concentrated in a comparatively small region at the center of the nebula and the lobes extend much further out. Measurements of Tylenda et al. (2003) give a size of $52'' \times 18''$ in Hα at the 10% level. However most of the emission comes from a much smaller region. As will be shown in the discussion of the radio emission measured by the VLA, most of the emission is coming from a region not more than $4''$ in size. The density in this region is quite high. The nebula is quite bright in radio continuum emission, being among the brightest PNe in the sky. The central star is faint and cannot be seen on this image, although it can be measured. As one of the few planetary nebulae (PNe) showing the Ne VI line, the exciting star is quite hot.

Hb 5 (PK 359.3-00.9) is, as the PK number indicates, located close to the galactic plane in the direction of the galactic center. As may be expected from a nebula in this direction, its extinction is very high. Its distance is uncertain. Statistical distances are between 0.7 kpc and 2 kpc (Acker et al. 1992). They also give an extinction distance of 2 kpc. A distance is computed by equating the ⟨rms⟩ density with the forbidden line density (computed below). A value of $d = 3$ kpc to $d = 7$ kpc is found which is considerably greater than the statistical distance. This is an indication that the nebula is intrinsically brighter than most PNe and may have evolved from a star of high mass. It is possible that this may be seen in the chemical abundances of the nebula.

Another important characteristic of this nebula is that the spectrum shows strong molecular hydrogen (H$_2$) emission. This is found in several other PNe as well (see e.g. Hora et al. 1999),

Fig. 1. The HST image of Hb 5. The width of the image is about $60''$. North is roughly in the direction from the center of the nebula to the brightest star outside the nebula.

but in Hb 5 it has a very strong intensity relative to the hydrogen lines. It is unlikely that these lines are formed in the same region which produces the high ionization lines. The simplest possibility is that they are formed in a photodissociation region (PDR) immediately surrounding the nebula. While other geometries may be possible, they are more complicated and we do not introduce them here. It is also very likely that some of the far-IR fine structure lines are formed in such a region and therefore consideration of a PDR in the analysis is a necessity.

The basic purpose of this paper is to explain the observed spectrum. This is done both in order to obtain accurate

---

abundances for this nebula and to quantitatively explain the presence of the molecular (H$_2$) lines. This is achieved in two ways. First by including the ISO spectra. The reasons for this have been discussed in earlier papers (e.g. see Pottasch & Beintema 1999; Pottasch et al. 2000, 2001; Bernard Salas et al. 2001), and can be summarized as follows.

The most important advantage is that the infrared lines originate from very low energy levels and thus give an abundance which is not sensitive to the temperature in the nebula, nor to possible temperature fluctuations. Furthermore, when a line originating from a high-lying energy level in the same ion is observed, it is possible to determine an effective temperature at which the lines in that particular ion are formed. When the effective temperature for many ions can be determined, it is possible to make a plot of effective temperature against ionization potential, which can be used to determine the effective temperature for ions for which only lines originating from a high energy level are observed. Use of an effective electron temperature takes into account the fact that ions are formed in different regions of the nebula. At the same time possible temperature fluctuations are taken into account.

Use of the ISO spectra have further advantages. One of them is that the number of observed ions used in the abundance analysis is approximately doubled, which removes the need for using large "Ionization Correction Factors", thus substantially lowering the uncertainty in the abundance. A further advantage is that the extinction in the infrared is almost negligible, eliminating the need to include large correction factors.

The second method of improving the abundances is by using a nebular model to determine them. This has several advantages. First it provides a physical basis for the electron temperature determination. Secondly it permits abundance determination for elements which are observed in only one, or a limited number of ionic stages. A further advantage of modeling is that it provides information on the central star and other properties of the nebula. We have included dust grains and molecules in the modeling and the computations include a state-of-art model atmosphere of the CSPN, the nebular shell, then a neutral zone and finally the PDR, all in a single model (i.e., an end-to-end model) for the first time.

A disadvantage of modeling is that there are possibly more unknowns than observations and some assumptions must be made. For example, concerning the geometry; we will assume that the nebula is spherical and that no clumping exists. The observed circular form in the radio maps (see Phillips & Mampaso 1988) and smooth emission within this inner region make these assumptions plausible. Other assumptions are discussed in Sect. 4.

This paper is structured as follows. First the spectrum of Hb 5 is discussed (in Sect. 2). Section 3 discusses the simple approach to determining the chemical composition and presents the resultant abundances. In Sect. 4, comparison with other abundance determinations is done along with a brief discussion on the errors. Section 5 gives a preliminary estimate of the T_{eff} of the CSPN. The model is presented after various relevant aspects about the method, inclusion of the PDR etc., are discussed, in Sect. 6. In Sect. 7, a discussion of the results is presented. Section 7.4 presents the details of the model PDR and discusses the important insights we derived from it. Section 7.5 looks at the whole picture emerging from modeling in a critical way, and provides a road map for the future. Details of the interesting insights obtained from the model are given in Sect. 8 and the evolutionary state of the CSPN is discussed in Sect. 9. Finally our conclusions are given in Sect. 10.

2. The spectrum of Hb 5

2.1. ISO observations

Observations were made on Hb 5 by ISO on 24 March 1997. Three observations were made. A short wavelength SWS01 complete spectral scan lasting 3450 s. was made centered at RA(2000) 17^{h}47^{m}56.04^s and Dec(2000) −29°59′40″, which is very close to the nebula center, which is given as RA(2000) 17^{h}47^{m}56.187^s and Dec(2000) −29°59′41.91″ by Kerber et al. (2003). It is known as TDT49400104. Because of the length of the exposure many faint lines are visible. There is also a long-wave spectral scan LWS01 (TDT49400105) at approximately the same position, and a longwave spectrum (TDT49400106) of a region 168 arcsec distant, which is used as the background spectrum because it is outside the nebula. Both of the longwave observations lasted 604 s. The diaphragm used for the short-wave observation was 14″ × 20″ below 12 μm, 14″ × 27″ between 12 μm and 29 μm and 20″ × 33″ above this wavelength. The entire nebula probably fit within the diaphragm in the entire wavelength range, and it is possible to check this by comparing the measured hydrogen line strengths with those expected from the radio continuum measurements. The diaphragm for the longwave measurements was considerably larger, about 80″ in diameter.

The resultant line strengths are shown in Table 1. The error in the intensities measured for the stronger lines is probably better than 10% while for the fainter lines the uncertainty increases to about 30% for the weakest lines. In the third column of the table (Intens.1) the measured intensities are given while in the fourth column (Intens.2) the measured intensities have been corrected for extinction using the extinction curve given by Fluks et al. (1994). The extinction corrections are usually less than 15%. For most nebulae we have ignored extinction in this spectral region, but this nebula has unusually high extinction.

2.2. Extinction

There are several methods for obtaining the extinction: (1) comparison of radio emission with Hβ flux, (2) comparison of observed and theoretical Balmer decrement, (3) dip at λ2200 Å, (4) photometry of the exciting star. Only the first two cases are realistic for Hb 5. First we will discuss the radio emission and the Hβ flux.

2.2.1. The 6 cm radio emission

The most reliable measurements of radio emission have been made by Phillips & Mampaso (1988) using the VLA. The integrated emission at 6 cm (the flux density) is 471 mJy. At 2 cm it is 428 mJy which would predict a 6 cm flux density of 482 mJy. At 21 cm a value of 289 mJy is measured and it is clearly optically thick at this wavelength. A single dish measurement has also been made by Milne & Aller (1982) using the Parkes telescope. They find a flux density at 6 cm of 548 mJy. This is slightly higher than the VLA measurement but the Parkes telescope has a beam of 4.5′ at half power. Since the measurement is made very close to the galactic plane there could be substantial contamination. Even so, if we use a value of 482 mJy for the 6 cm flux density, very little radiation could have been missed. Phillips & Mampaso give a diameter of about 3 to 3.5″ for the half-power size of Hb 5.

Table 1. ISO observations of Hb 5 (in units of 10^{-12} erg cm^{-2} s^{-1}).

Ident.	$\lambda(\mu m)$	Intens.(1)	Intens.(2)
H I 6-4	2.626	3.99	4.69
H$_2$	2.802	0.85:	0.98:
He II 7-6	3.091	1.95	2.23
H$_2$	3.234	0.57	0.65
H I 9-5	3.296	0.37:	0.43:
H I 8-5	3.739	0.97	1.04
H I	4.052	7.49	8.06
[Mg IV]	4.486	5.50	5.84
[Ar VI]	4.529	29.7	31.5
[Fe II]	5.340	3.55	3.72
[Mg V]	5.610	26.2	27.2
[Ar II]	6.985	14.2	14.6
[Na III]	7.318	3.09	3.20
H I 6-5	7.460	2.64	2.74
[Ne VI]	7.652	167.	174.
[Fe VII]	7.814	0.95	1.00
[Ar V]	7.902	11.8	12.4
[Na VI]	8.609	1.62	1.81
[Ar III]	8.991	29.8	34.5
[Na IV]	9.042	1.85	2.16
[Fe VII]	9.525	2.17	2.61
H$_2$	9.665	2.02	2.46
[S IV]	10.510	46.3	53.6
[Ne II]	12.812	36.4	38.7
[Ar V]	13.101	9.15	9.65
[Mg V]	13.519	1.55	1.63
[Ne V]	14.321	300.	314.
[Ne III]	15.554	199.	210.
[Fe II]	17.935	1.58:	1.7:
[S III]	18.711	21.6	23.1
[Ar III]	21.827	1.47	1.55
[Fe III]	22.926	0.76	0.79
[Ne V]	24.316	139.	145.
[O IV]	25.888	222.	231.
[Fe II]	25.983	3.67	3.75
[S III]	33.476	6.15	6.3
[Si II]	34.81	13.6	14.0
[Ne III]	36.01	15.4	15.8
[O III]	51.833	56.2	56.2
[N III]	57.329	28.5	28.5
[O I]	63.181	99.0	92.0*
[O III]	88.355	19.1	19.1
[N II]	121.861	3.83	2.35*
[O I]	145.464	4.45	≤4.4*
[C II]	157.719	25.7	≤5.0*

Intensity(1) is the measured intensity. Intensity(2) is the measured intensity corrected for extinction.
* Correction made for background emission (TDT49400106)
: indicates uncertain value.

2.2.2. The Hβ flux

The Hβ flux measured by O'Dell, 1963 is 3.0×10^{-12} erg cm^{-2} s^{-1}. Since the radio measurement of 482 mJy predicts a value of 1.19×10^{-10} erg cm^{-2} s^{-1}, the extinction value is $C = 1.60$ at Hβ. This is quite a large extinction and explains why IUE measurements in the ultraviolet were unsuccessful. It is not so unexpected in the direction of the galactic center. The extinction in terms of E_{B-V} is 1.09. This value, together with the extinction curve of Fluks et al. (1994), will be used throughout this paper. It has already been used to correct the ISO fluxes given in Table 1.

The Hβ flux may also be found by combining the hydrogen line intensities in the ISO measurements with the theoretical

Table 2. Hb 5: hydrogen line intensities (in units of 10^{-12} erg cm^{-2} s^{-1}).

$\lambda(\mu m)$	Transit.	Observ.	Corr.	Theory
4.052	Brα(5–4)	7.49	8.06	122.
2.626	Brβ(6–4)	3.99	4.69	111.
7.457	Pfα(6–5)	2.64	2.74	121.
3.739	Pfγ(8–5)	0.97	1.04	107.

The theoretical values of Hβ are assuming an electron temperature for hydrogen of $T_e = 12\,500$ K.

hydrogen line intensity ratios given by Hummer & Storey (1987). The results are shown in Table 2, where the predicted value of Hβ is given in the last column. This value agrees quite well with the value of Hβ derived from the radio measurements, which is a confirmation that essentially all the emission is observed in the ISO diaphragm.

2.3. The visual spectrum

The visual spectrum has been measured by a number of authors. All authors determine the extinction by trying to obtain the correct Balmer decrement but all obtain somewhat different extinction values. The most reliable spectra are those of Exter et al. (2004). In Table 3 we reproduce their results together with those of Acker et al. (1991) and those of Aller & Keyes (1987). The intensities shown in the table have been corrected for extinction by the authors themselves. We use these intensities even though different extinction corrections have been used ($C = 1.69$, 1.98 and 2.28 respectively) because in each case the correct Balmer decrement is then produced. This must mean that the flux calibration of each group was somewhat different, and somewhat incorrect. The use of the authors own extinction correction will correct at least some of the incorrect flux calibration. This will be correct in the neighborhood of the Balmer lines but uncertainties exist in other parts of the spectrum. We give most weight to the measurements of Exter et al. (2004) since they find a Balmer decrement extinction which is close to the extinction we find from the radio-Hβ method. The spectra of the other authors are primarily used for measurements in the infrared and for weak lines not measured by Exter et al. For the [Ne V] line at $\lambda3425$ Å only measurements by Aller & Keyes are available. Because these authors have probably over corrected for extinction we use a lower intensity for this line than they give. This indicates the uncertainty in the intensity of this line.

3. Chemical composition of Hb 5 from simplified analysis

The method of analysis is the same as used in the papers cited in the introduction. First the electron density and temperature as function of the ionization potential are determined. Then the ionic abundances are determined, using density and temperature appropriate for the ion under consideration, together with Eq. (1). Then the element abundances are found for those elements in which a sufficient number of ionization stages if not all, have been covered.

3.1. Electron density

The ions used to determine N_e are listed in the first column of Table 4. The ionization potential required to reach that ionization stage, and the wavelengths of the lines used, are given in Cols. 2 and 3 of the table. Note that the wavelength units are Å

Table 3. Visual Spectrum of Hb 5 (Intensities are normalized to Hβ = 100; They have been unreddened by each individual observer so as to obtain the correct Balmer decrement for his/her observations; the extinction used by each is not the same).

λ (Å)	Ion	Intensities			Average Intens.
		Exter	Acker	Aller	
3425	[Ne V]			161.	120.
3727	[O II]	76.4		62.3	70.
3869	[Ne III]	78.6	53.8	120.	80.
4068	[S II]	9.44			9.4
4076	[S II]	3.19			3.2
4102	Hδ	25.9		28.9	25.9
4267	C II				≤2.5
4340	Hγ	46.5	44.1	42.7	46.0
4363	[O III]	26.5	27.9	24.6	26.0
4471	He I	3.69		3.7	3.7
4686	He II	54.5	62.6	65.0	61.0
4711	[Ar IV]	10.1		9.8	10.0
4725	[Ne IV]	2.75		1.2	1.8
4740	[Ar IV]			18.5	18.5
4861	Hβ	100	100	100	100
5007	[O III]	1759.		1888.	1850.
5200	[N I]	8.2		3.66	7.1
5411	He II	4.43		5.06	4.6
5518	[Cl III]	0.96		0.7	0.96
5538	[Cl III]	1.65		1.2	1.65
5722	[Fe VII]			0.95	0.95
5755	[N II]	12.8	10.4	11.3	12.5
5876	He I	11.5	10.7	12.1	11.5
6312	[S III]	3.53		1.8	3.2
6435	[Ar IV]	2.26		3.4	2.4
6563	Hα	287	285	281	285
6584	[N II]	744.	318.	379.	700.
6717	[S II]	21.1		5.2	21.1
6731	[S II]	33.4		9.9	33.4
7136	[Ar III]	69.5	35.9		58.
7239	[Ar IV]			0.41	0.55
7325	[O II]	39.2	22.1	19.8	26.
7530	[Cl IV]			0.42	0.55
8046	[Cl IV]			1.2	1.5

Table 4. Electron density indicators in Hb 5.

Ion	Ioniz. Pot. (eV)	Lines Used	Observed Ratio	N_e (cm^{-3})
[S II]	10.4	6731/6716	1.80	6000
[S III]	23.3	33.5/18.7	0.27	8000
[Cl III]	23.8	5538/5518	1.72	10 000
[Ar III]	27.6	21.8/8.99	0.044	40 000
[Ar IV]	40.9	4740/4711	1.85	16 000
[Ne III]	41.1	15.5/36.0	13.3	9000
[Ar V]	60.0	13.1/7.90	0.75	20 000
[Ne V]	97.0	24.3/14.3	0.462	7500

when 4 ciphers are given and microns when 3 ciphers are shown. The observed ratio of the lines is given in the fourth column; the corresponding N_e is given in the fifth column. The temperature used is discussed in the following section, but is unimportant since these line ratios are essentially determined by the density. The [Ne III] and [Ne V] infrared line ratios sometimes give impossible values of density in other nebulae.

The electron density appears to vary quite a bit. It is difficult to judge whether this is a real variation or is caused by observational uncertainties. A value of between 10 000 and 15 000 cm^{-3} seems to be an average value. We have used a value of 12 000 cm^{-3} in calculating ionic abundances. There is a slight

Table 5. Electron temperature indicators in Hb 5.

Ion	Ioniz. Pot. (eV)	Lines Used	Observed Ratio	T_e (K)
[N II]	14.5	5755/6584	0.0179	9000
[S III]	23.3	6312/18.7	0.165	15 000
[Ar III]	27.6	7136/8.99	2.00	14 800
[O III]	35.1	4363/5007	0.0141	13 000
[O III]	35.1	5007/51.7	39.2	12 800
[Ne III]	41.0	3868/15.5	0.453	9200
[Ne V]	97.1	3425/24.3	0.985	17 000

indication that the electron density varies with ionization potential in a systematic way, such that lower densities are found at lower ionization potentials, thus further out in the nebula. It is interesting to compare this value of the density with the rms density found from the Hβ line. This depends on the distance of the nebula which is not accurately known, and on the angular size of the nebula, another rather uncertain quantity. Because of the distance uncertainty, we shall turn the calculation around, and compute what the distance will be for an ⟨rms⟩ density of 15 000 cm^{-3} in a sphere of radius 2″, that emits the Hβ flux given above. This yields a distance of 6 kpc. This value seems high and is quite uncertain but it does indicate that the "statistical distance" may be too low.

3.2. Electron temperature

A number of ions have lines originating from energy levels far enough apart that their ratio is sensitive to the electron temperature. These are listed in Table 5, which is arranged similarly to the previous table. A value of N_e = 10 000 cm^{-3} has been used. The electron temperature shows some scatter. There is some indication that for the lowest ionization potential a slightly lower electron density would be appropriate. The Ne III temperature is low, but that occurs rather often in other nebulae for a reason not understood. The Ne V temperature is high but the intensity of the line at λ3425 Å is uncertain. We have chosen to use an electron temperature between T_e = 13 000 K and 16 000 K with increasing ionization potential except for the lowest ionization potential for which a value of 9000 K is used.

3.3. Ionic and element abundances

The ionic abundances have been determined using the following equation:

$$\frac{N_{ion}}{N_p} = \frac{I_{ion}}{I_{H_\beta}} N_e \frac{\lambda_{ul}}{\lambda_{H_\beta}} \frac{\alpha_{H_\beta}}{A_{ul}} \left(\frac{N_u}{N_{ion}} \right)^{-1} \tag{1}$$

where I_{ion}/I_{H_β} is the measured intensity of the ionic line compared to Hβ, N_p is the density of ionized hydrogen, λ_{ul} is the wavelength of this line, λ_{H_β} is the wavelength of Hβ, α_{H_β} is the effective recombination coefficient for Hβ, A_{ul} is the Einstein spontaneous transition rate for the line, and N_u/N_{ion} is the ratio of the population of the level from which the line originates to the total population of the ion. This ratio has been determined using a model five level atom.

The results are given in Table 6, where the first column lists the ion concerned, and the second column the line used for the abundance determination. The third column gives the intensity of the line used relative to Hβ = 100. The fourth column gives the value of electron temperature used and the fifth column is the ionic abundances. The sixth column is the Ionization Correction

Table 6. Ionic concentrations and chemical abundances in Hb 5. Wavelength in Angstrom for all values of λ above 1000, otherwise in μm.

Ion	λ	I	T	N_{ion}/N_p	ICF	$N_{el.}/N_p$
He$^+$	5875	11.5	12 000	0.069		
He^{++}	4686	61.	14 500	0.054	1	0.123
N$^+$	6584	7.0	9000	1.34(−4)		
N$^+$	121.8	2.86	9000	3.87(−4)		
N^{++}	57.3	24.	14 000	2.09(−4)	1.9	8.4(−4)
O$^+$	3727	70.	9000	7.06(−5)		
O^{++}	5007	1850.	14 000	2.42(−4)		
O^{++}	51.8	47.1	14 000	2.40(−4)		
O^{+3}	25.8	194.	15 000	9.5(−5)	1.2	5.0(−4)
Ne$^+$	12.8	32.5	12 000	3.53(−5)		
Ne^{++}	15.5	61.4	14 000	3.83(−5)		
Ne^{++}	3869	80.0	14 000	7.56(−5)		
Ne^{+3}	4725	1.8	15 000	5.07(−5)		
Ne^{+4}	24.3	122.	15 000	2.45(−5)		
Ne^{+4}	14.3	264.	15 000	2.48(−5)		
Ne^{+5}	7.65	146.	16 500	4.88(−6)	1	2.2(−4)
S$^+$	6731	3.34	9000	2.77(−6)		
S^{++}	6312	3.2	13 000	2.35(−6)		
S^{++}	18.7	19.4	13 000	2.48(−6)		
S^{+3}	10.5	45.	14 000	1.45(−6)	1.5	1.1(−5)
Ar$^+$	6.99	11.6	10 000	9.85(−7)		
Ar^{++}	8.99	29.	14 000	2.44(−6)		
Ar^{++}	7135	58.	14 000	2.57(−6)		
Ar^{+3}	4740	18.5	15 000	1.48(−6)		
Ar^{+4}	7.90	10.4	15 000	3.63(−7)		
Ar^{+4}	7005	7.2	15 000	6.26(−7)		
Ar^{+5}	4.53	26.5	16 000	5.07(−7)	1	6.0(−6)
Cl^{++}	5538	1.65	13 000	9.74(−8)		
Cl^{+3}	8046	1.5	14 000	6.65(−8)	1.6	2.8(−7)
Fe$^+$	26.0	2.94	9000	7.35(−7)		
Fe^{++}	22.9	0.54	9000	1.34(−7)		
Fe^{+6}	9.52	1.9	16 000	7.48(−7)	2.2	4.0(−6)
Mg^{+3}	4.49	4.91	16 000	1.82(−6)		
Mg^{+4}	5.61	22.9	16 000	4.71(−6)	2.6	1.7(−5):
Na^{++}	7.32	2.69	15 000	1.48(−6)		
Na^{+3}	9.04	1.82	16 000	5.93(−7)		
Na^{+5}	8.61	1.52	16 000	1.93(−7)	1.4	3.2(−6)

I: Intensity given w.r.t. Hβ = 100.

Factor (ICF), which has been determined empirically. Notice that the ICF is unity only for neon, helium and argon for which all important stages of ionization have been measured. The ICF for oxygen was determined by assuming O^{+4} has the same abundance as O^{+3} as will be shown in the model. The ICF for nitrogen has been determined by assuming that the ratio of N^{++} to the total nitrogen abundance is the same as the ratio of Ne^{++} to the total neon abundance. This result is consistent with what has been found in other PNe for which IUE spectra are available so that the higher stages of ionization of nitrogen are directly measurable. This equality is also found in the model to be presented in Sect. 6. The ICFs for the other elements given are also found with the aid of the model. The abundance of carbon is not given because there is no suitable line. The abundances are determined to within 30 to 40% since the temperature uncertainty does not play an important role for the infrared lines.

4. Comparison with other abundance determinations

Table 7 shows a comparison of our abundances with the most important determinations in the past 20 years. There is marginal

Table 7. Comparison of abundances in Hb 5.

Elem.	Present	Exter(1)	Aller(2)	Solar(3)
He	0.123	0.141	0.145	0.085
N(−4)	8.4	12.3	11.5	0.60
O(−4)	5.0	3.9	6.6	4.6
Ne(−4)	2.2	4.1	1.2	1.2
S(−6)	11.0	6.7	8.9	14.
Ar(−6)	6.0	5.6	10.0	4.2
Mg(−5)	1.7			3.4
Na(−6)	3.2			1.5
Fe(−6)	4.0			28.
Cl(−7)	2.8		4.0	3.2

(1) Exter et al. (2004); (2) Aller & Keyes (1987); (3) Solar: Asplund et al. (2005).

agreement, usually to within a factor of two. A comparison is also made with the solar abundance (Asplund et al. 2005) for all elements except neon and argon). These last two elements have been discussed by Pottasch & Bernard-Salas (2006) and are essentially taken from the neon to magnesium ratio found by Feldman & Widing (2003) and the magnesium to hydrogen ratio given by Asplund et al.

The helium abundance has been derived using the theoretical work of Benjamin et al. (1999). For recombination of singly ionized helium, most weight is given to the λ5875 Å line, because the theoretical determination of this line is the most reliable. The abundance of helium is slightly lower than previous determinations due to their inclusion of the λ6678 Å line which we consider unreliable.

The nitrogen abundance is somewhat lower than earlier determinations. It is a better determination, because the N^{++} ion, which is the principle ionization stage, was only estimated in the earlier work and in the far infrared it is measurable. The nitrogen abundance is still more than ten times solar. Iron is much less abundant than it is in the sun as it is in most nebulae where it can be measured. Presumably it has been converted into "dust". It is rather uncertain because only three ionization stages have been measured. Magnesium appears less abundant than in the sun, but again its abundance is uncertain. The other elements are more or less solar.

4.1. Errors

It is difficult to determine the errors in the abundance determination. The reason for this is the following. The error can occur at several stages in the determination. An error can occur in the intensity determination and this can be specified: it is probably less than 30% and probably is lower for the stronger lines. An error may occur in correcting for the extinction, either because the extinction is incorrect or the average reddening law is not applicable. We have tried to minimize this possibility by making use of known atomic constants to relate the various parts of the spectrum. Thus the ratio of the infrared spectrum to the visible spectrum is fixed by the ratio of Brα to Hβ which is essentially an atomic constant, since it is almost independent of temperature and density for the values of these quantities of interest in this nebula..

A further error is introduced by the correction for unseen stages of ionization. This varies with the element, but is usually small because very many ionization stages are observed. Thus for neon all but neutral neon is observed, so that the error is negligible. This is also true for argon and to a lesser extent for

oxygen. For nitrogen and sulfur higher stages of ionization which do contribute somewhat to the abundance.

There is also an error due to an incorrect determination of the electron temperature. This is very small for ions represented by infrared lines, so that the abundances of neon, argon and sulfur will not be affected. The other elements are also less affected than when only the optical spectrum is available.

5. The central star

The central star has an uncertain observed blue magnitude of 18.6 (Tylenda et al. 2003). Corrected for extinction, $E_{B-V} = 1.09$, this is a blue magnitude of 14.2, a visual magnitude of 14.5, and leads to a hydrogen Zanstra temperature $T_z(\text{H}) = 100\,000$ K. The ionized helium Zanstra temperature is slightly higher $T_z(\text{HeII}) = 130\,000$ K. The value of the ratio of "forbidden line emission" (including all collisionally excited emission) to Hβ is about 35, but no ultraviolet lines have been observed and they usually make an important contribution. This indicates a lower limit to an energy balance temperature (T_{EB}) of $120\,000$ K. The presence of high ionization lines in the spectrum of the nebula, especially Ne^{+5}, probably indicates a somewhat higher temperature, possibly exceeding $150\,000$ K. If the star is at a distance of 3.2 kpc and has a temperature of $170\,000$ K, it will have a radius of $R = 0.17\,R_\odot$ and a luminosity of $L = 2 \times 10^4\,L_\odot$. We stress however that the stellar magnitude and the distance are only approximations so that the radius and luminosity are quite uncertain.

6. Model

6.1. End-to-end modeling

As mentioned earlier, in order to obtain as nearly a correct model as possible, the star, the nebula and a PDR must all be considered. The latter is important since we expect the observed molecular hydrogen lines to arise there. Let us first consider the star. There are several ways to obtain a reasonable estimate of the stellar temperature. Modeling the nebula-star complex will allow characterizing not only the central star's temperature but other stellar parameters as well (i.e., $\log g$ and luminosity). It can determine distance and other nebular properties, especially the composition, including the composition of elements which are represented by a single stage of ionization, which cannot be determined by the simplified analysis above.

The far-IR fine structure lines seen in the ISO spectra may be formed in the PDR (later we actually show the effect of not including the PDR on these lines), and hence this would have a bearing on the accuracy of the abundance determination since from our past experience with modeling other PNe, we found that a simple "star + nebular shell" structure in the model calculations could not produce these lines properly.

This method can take into account the presence of dust and molecules in the nebular material and elsewhere and thus is very comprehensive in approach. While the line ratio method is simple and fast, the ICFs rest on uncertain physics. To this end, modeling serves as an effective means and the whole set of parameters are determined in an unified way, assuring self consistency. Finally, this way one gets a good physical insight about the PN, the method and the observations.

It is with this in mind that we have constructed what we call an "end-to-end model" with the code Cloudy, using the latest version C06.02a (Ferland et al. 1998). To the best of our
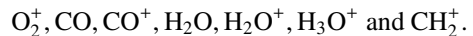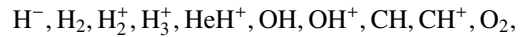
knowledge, this is the first time that a PN has been modelled in this way.

6.2. Photodissociation region, molecules, dust grains, and sources of non-stellar ionizing radiation in the nebula

We would like to briefly discuss about PDRs in general and then outline some details as to the implementation of this in Cloudy. Firstly although PDRs have been computed to interpret observations (particularly H$_2$), it should be noted that computing PDR spectra in an isolated way, which seems to be the prevailing culture, is unnatural in the sense that one always finds them in tandem with a PN or HII region or other host of astrophysical environs; for details of PDRs and their model computations, see the review by Hollenbach & Tielens (1997). Secondly, assuming an incident energy on the PDR and doing an isolated PDR modeling seems to be fraught with the danger of being arbitrary too since the incident energy is not known a priori, and often this is treated as a free-parameter to overcome this. Only an integral approach would be more realistic which is what we aim here.

We briefly give some details of the chemistry network in Cloudy here. Only a sketchy and generic description is possible. Cloudy has provision to consider a whole range of molecules commonly observed. Many details are available in the user manual, wherein all references to the literature are also cited. Since hydrogen molecule is perhaps the most important of all in many ways, the microphysics of this molecule has been exhaustively treated in the code, and details of this are available in Shaw et al. (2005); this paper too has relevant references to the chemistry network in Cloudy. The model H$_2$ molecule in Cloudy is so extensive that it altogether comprises a whopping number of 1893 levels capable of producing 524 387 lines. Also, one can find examples of self-consistent treatment of many prominent molecules in HII regions with inclusion of PDRs in the work by Abel et al. (2005) using Cloudy.

Once included, molecules are considered in all regions starting from the inner edge to the outer edge of the model and not necessarily in the PDR alone. The ion-molecule network includes among others

$$\text{H}^-, \text{H}_2, \text{H}_2^+, \text{H}_3^+, \text{HeH}^+, \text{OH}, \text{OH}^+, \text{CH}, \text{CH}^+, \text{O}_2,$$

$$\text{O}_2^+, \text{CO}, \text{CO}^+, \text{H}_2\text{O}, \text{H}_2\text{O}^+, \text{H}_3\text{O}^+ \text{ and } \text{CH}_2^+.$$

The hydrogen density therefore is given by

$$n(\text{H}) = n(\text{H}^0) + n(\text{H}^+) + 2n(\text{H}_2) + \sum_{\text{other}} n(\text{H}_{\text{other}})[\text{cm}^{-3}]. \qquad (2)$$

The formation and destruction rates of all processes (barring ones that have negligible rates) under statistical equilibrium conditions decide the number density of each specie at any point in the nebula. Approximately 1000 reactions involving 66 species of H, He, C, N, O, Si, S are treated in the chemistry network of Cloudy. The molecular heating and cooling mechanisms are duly introduced in the thermal balance. The population of H$^-$ in nebular conditions is very small but the opacity due to it can be dominant in the optical and near IR regions. It can aid in the formation of H$_2$ molecules significantly depending on the physico-chemical conditions. It should be noted that Cloudy's PDR calculations are well tested and agree well with other PDR models.

In a model which includes the presence of molecules, the presence of grains if introduced, can play an important role in

the gas-grain interactions and these are treated in considerable detail in Cloudy. H_2 molecular formation on the grain surfaces is a dominant process depending on conditions. The photodissociation of H_2 molecules by UV photons of energy between ≥ 11.2 and ≤ 13.6 eV (the "Solomon process") could be significant too; but grains can absorb these photons and thus reduce/prevent it. Electron temperature determination also involves gas-grain thermal exchanges.

From the available literature on Hb 5, we find that the IRAS measured fluxes in the 12, 25, 60 and 100 μm bands are substantial indicating that a large number of dust grains are present. The uncorrected flux densities in these bands are respectively 11.7, 79.2, 134.5 and 311.8 Jy. The peak in the region around 100 μm is a rough indicator of a cool dust at about 30 K. Emission features of PAHs (Poly Aromatic Hydrocarbon) have been observed with ISO by Peeters et al. (2002). Therefore we have included grains also in the modeling.

In addition to using the model atmosphere fluxes from Rauch (2003) for the CSPN, we also introduced the cosmic ray background radiation as additional ionizing source. That apart, there could be Galactic (general) background radiation too playing a role; but we ruled this out for the case of Hb 5 since it is embedded in the central disk, close to the galactic center. Due to the high density of interstellar matter expected, it is reasonable to expect the quantum of the background radiation to be insignificant. We note that these background radiation sources should be considered if one is computing a PDR.

6.3. Geometry

Hb 5 presents a bipolar geometry in the HST image (Fig. 1). There are other 2-D images extracted from long slit spectra presented in the web-site of Melissa Rice[1]. These images are in He II 4686 Å, Hβ, S II 6717 Å and S II 6731 Å. From the first two of these four, one can see that there is a central compact region from where most of the optical emission lines arise. There is also a narrow-band 2.122 μm image of Hb 5 presented by Davis et al. (2003). They also present a continuum subtracted contour plot of this image. Based on these, we decided that it is preferable to use a spherical geometry for this PN with a PDR at the outer edge delimited by the 2.122 μm contour plot; this would be both conceptually simple and reasonably adequate as it can be sensibly assumed that most of the optical and ISO spectra arise within a centrally located spherical region, although the angular dimensions of Hb 5 as seen in the HST image are much larger. It must be noted that the radio observations mentioned earlier also support a smaller angular dimension for most of the emission.

6.4. Architecting an "end-to-end model"

We summarize some aspects of the nitty-gritty of building the model for Hb 5 here. Firstly we experimented with a constant density model but this did not work out and there was already some indication of variation of density across the nebula (see the earlier section on "electron density"). So we worked with a variable density map where the density varies radially, starting from a high value at the inner edge and gradually decreasing outward. This was fed in as a table and hence one could iterate with changes in the radial profile between successive runs. We found that the density maps of Melissa Rice given on the basis of S II lines were of limited help since the CSPN of Hb 5 being a hot

---

[1] www.ctio.noao.edu/REU/ctioreu_2004/
Projects2004/mrice/mrice_research.html

star one would expect sulphur to be in a much higher ionization stage in the interiors. See for example, our earlier modeling of Me 2−1 in Surendiranath et al. (2004), where we have shown the ionization structure in Fig. 8. We note that the radial variation considered is within the spherical region modelled.

Regarding dust grains, we experimented with a variety of grains like those typically seen in ISM, pure silicates, pure graphites and PAHs, but we tried only single sized grains in all cases. As we progressed, we changed over to a variable dust density map instead of using a fixed dust to gas ratio (at every radial point) with which we started. We had to experiment with a radial profile of the dust density as was the case with the gas density. It thus became a very complex exercise and computation times were long. Computation time per run depends on whether one included the stochastic heating (also known as quantum heating) of tiny grains. Inclusion would make it very time consuming. Here we have excluded it for the sake of simplicity of the model as well as economy of time.

Further down the path, we wondered whether the excitation of hydrogen molecules was due to shock or fluorescence; using the diagrams of Sternberg & Dalgarno (1989) (their Fig. 7a) and the observed ratio of 2.802 μm/3.234 μm (1.64), we perceived that perhaps high densities would be needed and shocks may not be needed. From the above-referred figure which gives the predicted H_2 spectrum, we calculated that at high densities one can get the ratio of H_2 lines 2.122 μm/2.248 μm as ~7. Davis et al. (2003) quote (their Table 3, Col. 3) the observed ratio of these lines for Hb 5 to be more than 10 in a region ~5 arcsec from the CSPN and based on their analysis which involves published shock and PDR models, conclude that both fluorescent and shock excitation may be important for Hb 5. Indeed, quite high nebular expansion velocities of ~250 km s^{-1} have been observed (see Corradi & Schwartz 1993 and Pishmish et al. 2000) and therefore shocks are not ruled out. But we decided to work with a rather simple static model and wanted to see whether we can reproduce the observed line fluxes from stellar and cosmic ray ionizing radiation. We found that getting the right H_2 densities in the PDR and exciting them to yield the desired flux levels in the ISO observed lines was difficult simultaneously with production of the right model spectrum that would match observations. Parameters of the CSPN had to be adjusted within a narrow range. And further, it became clear that there was a need to consider a neutral zone between the nebular (ionized) zone and the PDR. Thus, evolving ideas forced design changes to the original template which was relatively pedestrian. Our final model is presented in Table 8 and we discuss more about this below.

6.5. Results

The model we have presented as final had the input parameters shown in Table 8 and the corresponding output spectral fluxes are compared to the observed ones in Table 9. Figure 2 shows the gas and dust density radial profile used in the final model. In the appendix we give some predicted strong lines in UV region which may be useful for future comparison.

7. Discussion

After a large number of models were computed as discussed in the previous section, it became gradually clear that our final model can only be a heuristic model.

Table 8. Parameters representing the final model.

Parameter	Value			
Ionizing source				
Model atmosphere	Rauch			
$T_{\rm eff}$	171 500 K			
Log g	6.2			
Luminosity	6800 $L_{\odot}$			
+				
Cosmic ray background	H^0 ionization rate = $2.5 \times 10^{-17}\ S^{-1}$			
	H_2 ionization rate = $5 \times 10^{-17}\ S^{-1}$			
Nebular lobe				
Density n(H)	See Fig. 2			
Abundance	H	He	C	N
	12.000	11.121	8.875	9.130
	O	Ne	Na	Mg
	8.898	8.188	6.556	7.292
	Si	S	Cl	Ar
	7.079	7.146	5.570	6.820
	Fe			
	6.079			
Size	7″ (radial extent)			
Distance	3.20 kpc			
Dust Grains	Silicates of radius 0.010 μm (Fig. 2)			
inner radius	1.436e16 cm (~0.00465 pc, 0.3″)			
outer radius	3.351e17 cm (~0.108 pc, 7″)			
Filling factor	1.0			

## 7.1. Nebular density and temperature

The electron density and temperature as computed by our model is plotted in Fig. 3 against nebular depth, i.e., the radial distance calculated from the inner edge. There is a small but noticeable spurt in Te and Ne near the PDR (see a magnified view in Fig. 6). We discuss the significance of this later, when we come to the topic of the model PDR.

7.2. Comparison of model spectrum with observation

As mentioned earlier we have attempted to obtain a good match for 76 observed lines and these are shown in Table 9. The overall model spectrum seems to be at variance with observed spectrum though the match of the hydrogen and helium lines are good along with the match of the absolute Hβ flux.

All the diagnostic lines are not reproduced well by the model, and match for most of the heavy element lines in general is not satisfactory. We will look at some aspects of this later.

But we could achieve a good match for the H$_2$ lines as follows; we tried out several ideas over a large number of trial runs, including adding a secondary cooler companion to the CSPN. Since Hb 5 is a bipolar PN, the central source might be a binary star and the radiation from this secondary might be powering the PDR and particularly the hydrogen molecules. Adding a cooler companion did not work. We introduced a neutral zone between the ionized nebular zone and the PDR and suitably modified the gas and dust density maps (Fig. 2). Density maps (i.e., the radial profiles) were carefully carved out to bring out desired spectra and this necessitated increasing the value of the distance to the PN. Given the general idea of the gas density to be not more than about 2.0×10^4 (from the first part of this paper), it became necessary to increase the distance to reproduce the observed absolute Hβ flux too. This is an important constraint. We have experimented with a shorter distance between 1 and 2 kpc (which is roughly the statistical distance estimate) and found that this
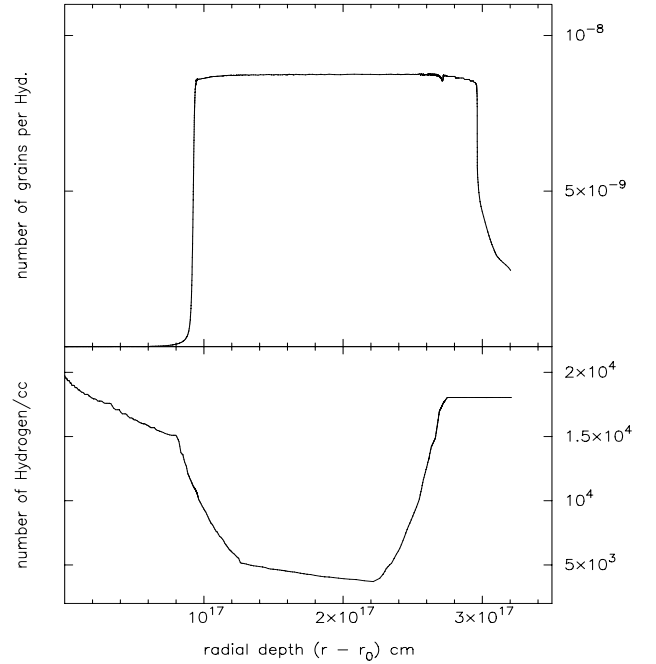
Fig. 2. Input density map for gas and dust; r_0 is the inner radius of the nebula. r is the radial distance from the CSPN.
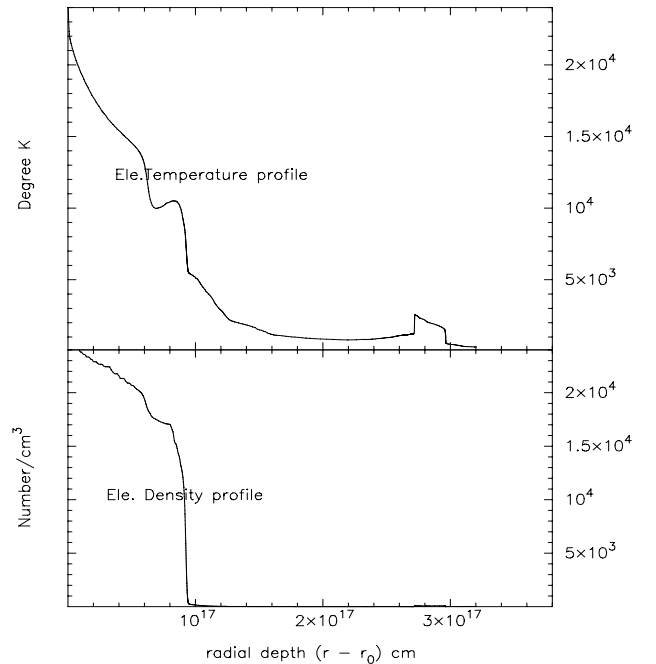
Fig. 3. $T_{\rm e}$ and $N_{\rm e}$ across the nebula; X-axis is radial depth (see Fig. 2).

would not work. This is mainly because the angular extent from where most of Hβ flux is coming is small and of course, the angular size of the molecular hydrogen zone measured from the 2.122 μm contours of Davis et al. (2003). There was a need for the neutral zone too. So to allow sufficient physical volume for all these, we had to increase the distance and we had gone up to 3.6 kpc and then later zeroed in on the value of 3.2 kpc given in Table 8. If the distance were to be much shorter, it would be more difficult to form a cool PDR at a shorter radial distance from a very hot CSPN; it might require more shielding grains. So our model distance seems very sensible. And this makes Hb 5 one of the very luminous PNe. And the hump in the gas density (Fig. 2)

Table 9. The emission line fluxes (Hβ = 100).

Label	line	Model flux	Obsd. flux (dereddened)	Label	line	Model flux	Obsd. flux (dereddened)
TOTL	4861A	100.00	100.00	H 1	3.740 m	1.01	0.88
Ne 5	3426A	173.98	120.00	H 1	4.051 m	7.65	6.72
TOTL	3727A	43.84	70.00	Mg 4	4.485 m	8.64	4.87
Ne 3	3869A	143.26	80.00	Ar 6	4.530 m	63.54	26.25
S II	4070A	5.93	9.40	Mg 5	5.610 m	17.20	22.67
S II	4078A	1.92	3.20	Ar 2	6.980 m	1.05	14.60
H 1	4102A	26.40	25.90	Na 3	7.320 m	2.87	2.69
H 1	4340A	47.46	46.00	H 1	7.458 m	2.40	2.30
TOTL	4363A	16.47	26.00	Ne 6	7.652 m	92.43	145.00
He 1	4471A	4.48	3.70	Fe 7	7.810 m	0.72	0.81
He 2	4686A	55.83	61.00	Ar 5	8.000 m	18.68	10.33
Ar 4	4711A	6.96	10.00	Na 6	8.611 m	0.77	1.51
Ne 4	4720A	0.90	1.80	Ar 3	9.000 m	25.95	28.75
Ar 4	4740A	15.31	18.50	Na 4	9.039 m	1.51	1.80
O 3	5007A	1712.92	1850.00	Fe 7	9.510 m	2.28	2.19
He 2	5412A	4.26	4.60	H2	9.662 m	1.79	2.05
Cl 3	5518A	0.57	0.96	S 4	10.51 m	112.67	44.67
Cl 3	5538A	1.19	1.65	Ne 2	12.81 m	1.80	32.25
Fe 7	5721A	0.99	0.95	Ar 5	13.10 m	15.23	8.11
N 2	5755A	7.82	12.50	Mg 5	13.52 m	1.39	1.37
He 1	5876A	12.79	11.50	Ne 5	14.32 m	250.91	261.67
O 1	6300A	3.52	35.00	Ne 3	15.55 m	137.16	175.00
S 3	6312A	2.68	3.20	Fe 2	17.94 m	0.15	1.43
Ar 5	6435A	4.58	2.40	S 3	18.67 m	20.45	19.25
N 2	6584A	379.11	700.00	Ar 3	21.83 m	1.42	1.30
S II	6716A	4.70	20.00	Ne 5	24.31 m	72.41	120.83
S II	6731A	9.33	35.00	O 4	25.88 m	131.96	192.50
Ar 5	7005A	9.82	7.20	Fe 2	25.99 m	0.47	3.15
Ar 3	7135A	35.76	58.00	S 3	33.47 m	3.10	5.29
Ar 4	7237A	0.32	0.55	Si 2	34.81 m	17.50	11.67
TOTL	7325A	9.60	26.00	Ne 3	36.01 m	9.60	13.17
Cl 4	7532A	0.68	0.55	O 3	51.80 m	40.23	47.20
Cl 4	8047A	1.36	1.50	N 3	57.21 m	31.86	24.00
H 1	2.625 m	4.36	3.90	O 1	63.17 m	36.17	77.30
H2	2.802 m	1.00	0.82	O 3	88.33 m	5.16	16.10
He 2	3.091 m	1.91	1.87	N 2	121.7 m	0.50	1.97
H2	3.234 m	0.64	0.55	O 1	145.5 m	4.99	≤3.7
H 1	3.296 m	0.70	0.36	C 2	157.6 m	7.34	≤4.2

Absolute Hβ flux(n.lobe) Model: 1.16×10^{-10} erg cm^{-2} s^{-1} Obsn: 1.19×10^{-10} erg cm^{-2} s^{-1}

Notes: "A" in col. "Line" signifies Angstrom; "m" signifies μm. In col. "Label", we have followed the notation used by Cloudy for atoms and ions; this will make identifying a line in Cloudy's huge line list easy. Neutral state is indicated by "1" and singly ionized state by "2" etc., 'TOTL' typically means the sum of all the lines in the doublet/multiplet; or it could mean sum of all processes: recombination, collisional excitation, and charge transfer. Some elements are represented by usual notation as per Cloudy.

was again carefully crafted to achieve the desired results. We discuss more on this again later, particularly the input density maps for gas and dust.

The mismatch of the far-IR fine structure lines between the model and the observation was a fall-out from which we could not escape. Far-IR lines of O I, C II, Si II, N II and Fe II are all off the mark. Table 10 provides an idea of the role played by the PDR in producing these lines. The dust radiation from the model could not match the observations. We discuss these in more detail later.

7.3. Central star

We stated above that absolute Hβ flux and line fluxes of H and He match well. It must be noted that the principal optical depth in a PN (with no dust in the ionized nebular shell) is caused by the elements H and He alone and so from the energetics point of view, this makes the model CSPN parameters seem reasonable. From our trial models it was found that the T_{eff} and log g

Table 10. Effect on line fluxes due to exclusion of PDR and cosmic ray background. Hβ = 100.

Label	line	model with PDR and cosmic ray	flux obsd	model without PDR	model without cosmic ray
H₂	2.802 m	1.00	0.82	0.00	1.14
H₂	3.234 m	0.64	0.55	0.00	0.71
H₂	9.662 m	1.79	2.05	0.00	2.23
Fe 2	17.94 m	0.14	1.43	0.12	0.15
Fe 2	25.99 m	0.47	2.92	0.11	0.50
Si 2	34.81 m	17.50	11.67	2.12	18.40
O 1	63.17 m	36.17	77.30	4.42	37.55
N 2	121.7 m	0.50	1.97	0.49	0.50
O 1	145.5 m	4.99	≤3.7	0.37	5.21
C 2	157.6 m	7.34	≤4.2	1.03	7.39

Note: all other lines and abs. Hβ have the same fluxes in all models. The "model with PDR and cosmic ray" is our final model of Table 8.
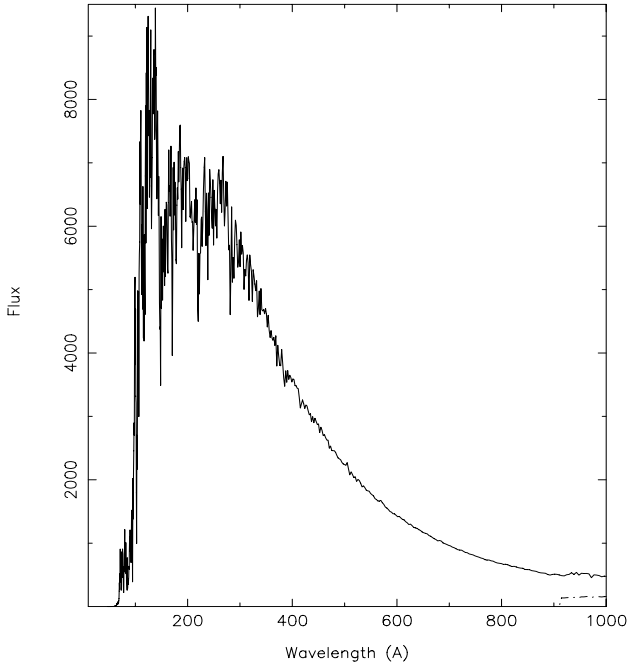
Fig. 4. Stellar ionizing radiation – Upper curve is the incident radiation; lower curve (broken line) at the bottom right of the panel beyond 912 Å shows the transmitted radiation (attenuated incident continuum) and does not include diffuse emission from the nebula.
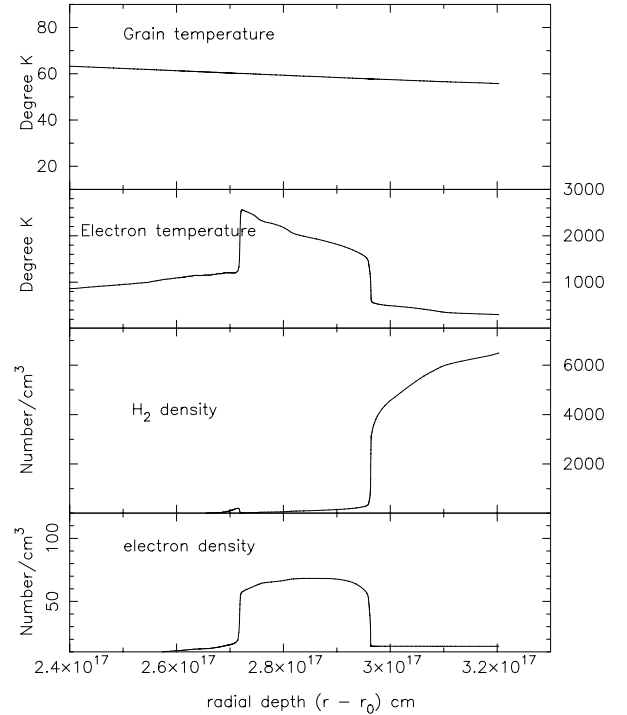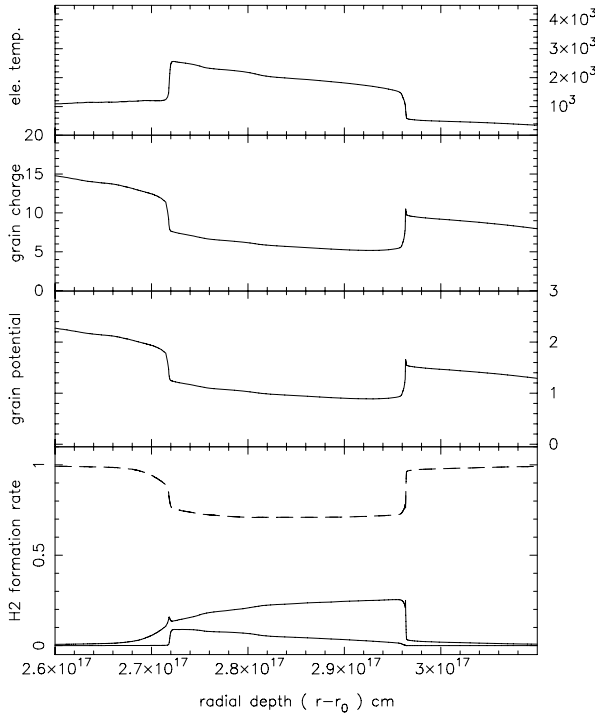

Fig. 5. H_2 formation mechanism in the PDR. The three curves in the bottommost panel give the fractional contribution by the three dominant mechanisms: top: formation on grain surface; middle and lower are due to other reactions explained in the text. The number given is the fractional contribution and the sum of all the contributions is taken as unity.

assigned in the final model are pretty good. Any change in them worsened the absolute Hβ flux and the lines from highly ionized elements. We also note that small changes in log g (as small as 0.1) can disturb the fluxes of H_2 lines.

Fig. 6. The formation of H_2.

Looking at the plot of the incident and transmitted energy curve (Fig. 4) the absorption below 912 Å is complete. The region longward of 912 Å is very important. The shape of the transmitted energy in the latter region matters most in the formation of sufficient column density of H_2 molecules in the PDR and correct reproduction of its lines measured with ISO. More on this in the section on PDR below.

7.4. The model PDR

We used the "large model of the H_2 molecule" in Cloudy for the model calculations. The formation of molecular hydrogen can be seen in the plots shown in Figs. 5 and 6. For better view, the plot is not from the inner edge of the nebula. We did not find any other molecule in sufficient numbers either in the PDR or in other regions in the model and so only H_2 is plotted. In addition to H_2 density, one can also see the Te and Ne plotted together. As can be clearly seen, there is a sudden spurt in the Te after it has been steady at a very low value in the neutral zone accompanied by a rise in Ne as well, and then Te gradually falls off; when the Te value reaches a critical level suitable for the formation of H_2, it can be seen that the H_2 density rises sharply. The maximum value of H_2 density indicates that about 5e+3 hydrogen atoms are in neutral state ($n(H^0)$ in Eq. (2)) near the end point. Our attempt to reduce the height of the bump in the $n(H)$ (Fig. 2), did not produce the desired H_2 emission.

As can be seen in the dust density map, the number of grains/cc present in the nebula is varied radially with a suitable formula:

$$\phi = (\text{constant}) \times [f1 \times A + f2 \times B] \qquad (3)$$

where $A = n(H^0)/n(H_{tot})$ & $B = n(H_2)/n(H_{tot})$ and "constant" is six times the default value of the number of grains per hydrogen for a chosen option in the model and, the quantity in the square bracket defines the variable "grnvrydpth" within Cloudy (refer

to user manual for details). $n(H_{tot})$ is the total number of hydrogen atoms in all forms given by Eq. (2). We experimented with variations in the two factors "f1" and "f2" and the final model had "f1" = 1.17 and "f2" = 0.0. Since the basic idea was to enhance the dust to gas ratio in the neutral zone and the PDR, other types of formulae may be possible.

We have analyzed the heating and cooling taking place in this zone by tabulating (not shown here) the fractional cooling and heating caused by various agents in the PDR. The dust density rises in the neutral zone immediately after the ionized zone at ~1.0e17 cm (depth). This helps to absorb the FUV photons of energy between ≥11.2 and ≤13.6 eV to reduce the impact of the Solomon process which can lead to part destruction of H_2 by photodissociation.

After this, farther in the radial distance, as one nears the PDR, there is a rise in the number of grains (this rise in the grain population is due to the steep rise (hump) in the inputted density map, $n(H)$ vs "r"). The cause of the sudden spurt in the Te near ~2.7e17 cm is basically the lowering of grain charge and potential in a somewhat abrupt manner (see upper part of Fig. 5). The grain charge is computed in Cloudy by the method discussed in detail by van Hoof et al. (2004) which essentially follows the physics in Weingartner & Draine (2001) with some modifications. The quantity plotted represents the mean average grain charge (in units of elementary charge) for a given grain bin (see details in the above references). The grains in our model are becoming positively charged as is typical in an ionized region. The grain potential differs from the grain charge in terms of constants only (grain charge, grain size;) and is given in units of eV. This lowering potential in turn leads to increased photoelectric emission leading to extra heating ("Ne" also rises due to this spurt in Te and our analysis of the model output shows that a substantial part of the rise in Ne is caused by H becoming H^+ as a result of the spurt in Te, rather than due to photoelectric emission) and this situation continues at a slowly decreasing rate till we reach ~3.0e17 cm where the $n(H)$ flattens out (see Fig. 2). Around this point the grain charge and potential rise up which result in less photoelectric heating thus lowering Te and when Te reaches around 1100 K, the formation rate of H_2 molecules on the grain surface increases at a high rate (Figs. 5 and 6) and the H_2 emission in the observed lines rise up. The formation rates plotted are relative contribution to the H_2 formation via different mechanisms. The number given is the fractional contribution and the sum of all contributions by all the methods is treated as unity. More description on this aspect and the plot follows later. Note also that the number of grains decreases at this point (Fig. 2) since the number of neutral hydrogen decreases (see Eq. (3)) as a result of increased H_2 formation. The grain temperature (T_g) is very critical in the matter of evaporation of the hydrogen atom from the grain surface before it can react to form H_2; T_g has to remain below ~75 K to reduce such losses. Looking at the top part of Fig. 6, it can be seen that it hovers around 60 K only. At about 2.963e17 cm, the grain charge goes up, the contribution of grain heating comes down (as also noted in the thermal balance analysis) and Te drops rather abruptly. So it is clear that the grain charge variation triggers both the rise and the fall in Te.

The spurt in Te is accompanied by the rise in O I 63 μm line emission, the Si II 34 μm line emission, the cooling of gas by grains (grain recombination cooling), and the cooling due to H_2 being excited (within the ground state) by collisions, which are major coolants. O I 145 μm and C II 157 μm also count as other coolants. The dominant role gets interchanged amongst the various major coolants as we go further in radial depth starting from ~2.7e17 cm. Beyond ~3.0e17 cm, as the Te falls lower, the H_2

formation takes place at a reduced rate and tapers off towards the end (the neutral hydrogen population is substantial in this outskirt; note the value given in the beginning of this subsection). The main heating agent in the PDR is the grain photoelectric heating (~98%). This is true of all the models we tested.

In one model, where we reduced the abundance of C by 25%, the abovementioned spurt in Te did not occur and the H_2 lines became very weak. The strength of the H_2 lines is sensitive to the abundance of Si also. We also note that in models where we could form H_2 in sufficient number at a shorter radial distance but at lower Te (compared to our final model's result shown in Fig. 6), weak H_2 lines were produced. So the electron temperature in the PDR has to be at an optimal value to get the H_2 emission right. Because of such delicate adjustments needed, we did not invoke the idea of depletion of refractive elements in our numerical experiments, although it should be done since the quantum of dust is very high in the finalized model. This means our final model abundances may not be very realistic. The hump in the gas density map looks quite realistic, since without it we were unable to get the H_2 formation and emission to match observation.

The most important physical insight derived from modeling is that the presence of dust grains in the neutral zone (in reducing the full impact of the destruction of H_2 by Solomon process) and in the PDR (in augmenting H_2 formation), plays a key role in getting the hydrogen molecules to form to the desired density and to emit the desired level of fluxes seen in the ISO observations. We had found from running a number of models that unless sufficient dust grains are added the H_2 lines do not budge easily and light up. We had earlier tried dust grains in all the regions from the inner edge to outer edge with the dust to gas ratio typical of PNe, but that did not work. We have seen models with sufficiently large number of H_2 molecules but with very weak emission in their lines. Only upon increasing the grain population enormously in the neutral zone and the PDR, (and making it practically nil in the ionized zone) we could get the H_2 lines really blazing. Thereupon by suitable tuning we obtained the final model. Adding a cooler companion star did not work nor adjusting any other parameter. We note here that the dust grains we considered were silicate grains of radius 0.010 μm. We had tried other types too; some models were tried with PAHs but we did not get encouraging results. As our internalized dust grain model was minimalistic, we did not compare dust radiation output with observations, namely, i) PAH emission features seen in ISO and ii) the IRAS band fluxes.

The mean dust to gas ratio by mass (as computed within the model) is 1.67e−2. We have estimated the total mass of the nebula using the density map as ≃2.19 $M_\odot$. (This neglects the mass in the heavy elements starting from C upwards.) Therefore the total dust mass in the nebula is ≃0.036 $M_\odot$! This is much higher than the typical dust mass expected in a PN. Generalizing this leads to a significant new speculative insight that PDRs may harbour lots of dust grains. The reason we believe that this may well be a generalized phenomenon is that in the PDR literature one finds that a number of workers have found models showing an emission deficit in H_2 lines compared to observations (see Habart et al. 2005). Enhanced dust to gas ratio in the PDR due to gas-grain drift is found to reproduce H_2 observations in the reflection nebula NGC 2023 in the work by Draine & Bertoldi (2000). We became aware of these works only after we independently hit upon the idea of enhancing dust grains in the neutral zone and the PDR to achieve desired emission level in H_2 lines. We note here that recently Klaas et al. (2006) have found
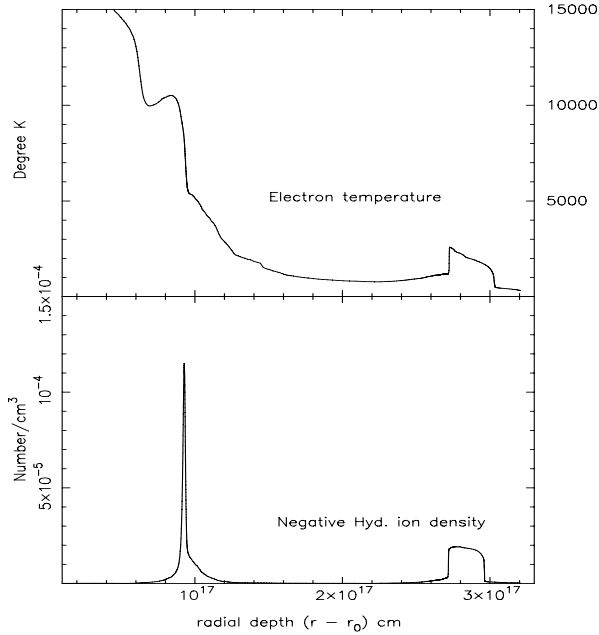
Fig. 7. The formation of H⁻.

similar high dust to gas ratio in NGC 7008 and so our value is not unusual.

The number densities of H⁻ are plotted in Fig. 7 along with Te. The densities are very negligible, but the density variations in the PDR region where Te spurts is interesting. In the bottom part of Fig. 5, the H_2 formation rate due to the three dominant mechanisms are shown. The three curves from top to bottom represent respectively the following: formation on grain surface, formation due to the reactions

$$CH^+ + H \rightarrow C^+ + H_2 \quad \text{and}$$

$$H + OH \rightarrow O + H_2.$$
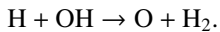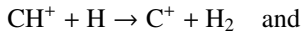
It is clear that formation on grain surface outperforms all other mechanisms and the mechanism via H⁻ (not shown) is very negligible.

About some reported CO observations (see Phillips et al. 1969 and Phillips & Mampaso 1992) on Hb 5: In general one needs to go farther in radial distance beyond the H_2 zone to get CO to form and start emitting. In the PDR literature the parameter A_v is used rather than radial distance and its value in our final model is 0.17. This is the value of the extinction due to the internal dust in the nebula. In our model, the observed H_2 emission image size delimited the end point of computation.

We find that the reported observations of CO in Hb 5 are presently too uncertain to consider them seriously here. There is a need to better reobserve Hb 5 in the CO lines.

7.5. Pointers

i) The final model did not reproduce diagnostic lines well barring a few exceptions. One pointer is that perhaps better quality atomic data have to be used. We have modelled several nebulae in this series of papers on abundances in PNe and found in each, that the neon lines (in the model) have always been somewhat erratic. So the situation here too might be caused by this factor. Similarly in the case of O II the reproduction of the doublet 3727 Å is bad; observations and detailed analysis by Wang et al. (2004) point that

Zeippen's (1982) old value is better for the transition probability in order to get good match. The version of Cloudy we used incorporates the recent values of Zeippen (1987). If a set of ions of one element is introduced with wrong atomic parameters, it can skew up the photon energy distribution within the ionized zone and further spoil correct portrayal of ionization/excitation structure of other ions too. This may be a serious problem. We found in Cloudy's web-site an assurance that future versions will have an option to introduce the old values of Zeippen (1982) for O II. The old values were used in the first part of this paper.

ii) The density distribution of gas and dust have been treated as unknowns and carefully modified to get desired results. But a more systematic way would be to use images in emission lines (see item vi below).

iii) We have been taking for granted that the ionizing energy distribution from the (CSPN) model atmosphere is an accurate portrayal of reality. Although there is no sufficient ground for us to doubt this (since it is a state-of-art model atmosphere), we have found that the EUV portion of the energy distribution can trigger a tizzy in the output spectrum if the "peaks and valleys" caused by sharp ionization edges, seen in that region are tinkered in small measure in the input. Since it is not possible to verify this portion of the energy distribution with observation, we would like to point out that such causes are also to be considered.

iv) As shown in Table 10, the model without the PDR zone reproduced some of the far-IR lines very poorly, i.e., they are all very weak in strength, and the H_2 lines are all completely destroyed. All other lines not shown in Table 10 had the same flux as our finalized model. Therefore this is a strong pointer to conclude that PN model of the future has to be an "end-to-end model".

v) Table 10 also shows the effect on the model when the cosmic ray background as additional ionizing source is not present. While only some H_2 lines are affected significantly (enhanced), the lines formed in the PDR have undergone very small changes. All other lines are unaffected.

vi) Another very important problem faced by the modeler is the lack of systematic and homogeneous observations. We have found, when trying to combine all available observations in the literature, that the set is inhomogeneous and not easily amenable to modeling. For example, the spectral fluxes need to be from the whole of the nebula; the calibration and splicing of joints have to be seamless between one region of wavelength to another and between different sets of data. Differences in apertures used have to be tackled. Radial distribution of density is another problem. Deconvolving the images may work out, but one has to have images in lines from desirable stages of ionization to cover all the parts of the PN modelled. And lastly but not least the distance is poorly known. Computationally a small fraction of a kpc will matter in terms of final numbers, but we know that estimates are uncertain by much larger values.

vii) Our model nebula's size is limited to a part of the observed nebula. Material beyond the outer edge of the model in the form of dust, ions and molecules is not considered. In particular we note that the simple spherical geometry (which neglects the extended lobes) and the possibility that some of the contribution to neutral and singly ionized lines as well as other PDR lines such as Fe II and Si II could arise in the lobes may be the reason for the model behaviour. Also it may be possible that H_2 pure rotational lines could be from extended lobes.

Some of these pointers (and other approximations and uncertainties already discussed) are the important reasons why our model does not give numerically usable results. Based on these issues as well as the insights we got about the PDR and the CSPN, we classify our final model as a heuristic model. It provides a road map for future work.

8. Some interesting possibilities with caveats

We list the significant insights we obtained from our modeling here; since these insights are derived from a heuristic model, they should be treated with caution.

i) Interpretation of molecular H_2 lines and far-IR fine structure lines in Hb 5 as observed by ISO necessitates inclusion of a photodissociation region self-consistently in a photoionization model. Radiation emanating from PDR can pass inward too, affecting the ionized zone, and Cloudy takes this into account. There could be "backwarming effects", depending upon conditions present. Retrofitting a separate PDR computation to a truncated photoionization model may lead to physically wrong results. Abundances determined from a model excluding the PDR may be incorrect since in addition to the above physical factors, strictly speaking "nebula" should mean all regions including the PDR.
Exclusion of cosmic ray background radiation can affect molecular hydrogen emission. If the ionized zone alone is used for abundance determination, the geometrical location of incidence of background radiation (other than cosmic rays), would not be properly treated. We note here that Cloudy does not implement a rigourous radiative transfer and it uses only an escape probability mechanism; it takes care of various kinds of background radiations including those that would matter for a PN in an intracluster medium in the extragalactic context, for example, in an approximate way (see user manual).

ii) Molecular H_2 emission from the PDR in the model Hb 5 is excited in a region filled with a large number of dust grains. Therefore the determination of the abundance of refractive elements needs a more thorough approach.

iii) It may be possible that a neutral zone is present between the ionized zone and the PDR in Hb 5, and this hosts lots of dust grains which play a benign role in the formation of H_2 molecules in the PDR.

iv) Dust grains are found to be the necessary ingredient for both the formation and emission of H_2 lines (to the level observed by ISO in Hb 5) on the basis of our modeling exercise. We could not achieve this by any other means we could try within the framework of our model. We however note that our work does not rule out the role of shocks.

v) On a more general speculative note it is expected that the "dust grain (silicates) – H_2 molecular synergy" may play an important role which needs exploration in future models of PDR, and in interpreting high H_2 emission in the Galactic and extragalactic contexts. One possibility is that the total amount (mass) of dust grains in the Galaxy may be underestimated since H_2 line emission is seen to be very strong in many locales. In the extragalactic context too this idea may be useful in explaining anomalous emission.

9. Evolutionary state

The abundances can be used to discuss the evolutionary state by comparing them to theoretical evolutionary models. The models given by Karakas (2003) are used to make this comparison. The most noticeable piece of information is the high N/O ratio. It has a value of about 1.5 and is one of the higher values measured. It indicates that "hot bottom burning" has taken place. This occurs in higher mass stars, indicating that Hb 5 originated from a star of higher than 4 $M_\odot$. There is no indication that oxygen has been depleted however, as is the case for the central stars of NGC 6302, Mz3 and NGC 6537, This probably eliminates stellar values higher than 5 $M_\odot$, placing a severe limit on the mass of the exciting star.

10. Conclusions

We have presented the ISO far infrared spectrum of Hb 5. Including the visual spectrum has enabled us to derive nebular abundances of ten elements using the ICF method. In addition, a detailed photoionization model that includes a neutral region and a photodissociation region (i.e., an end-to-end model) has been presented. Grains and molecules have been treated self-consistently in this procedure. As discussed earlier in detail, we conclude that this can only serve as a heuristic model. The model CSPN parameters and the distance seem very sensible, while the abundances are not reliable. We recommend the abundances from the ICF method for Hb 5. These are given in Table 7.

More observations and computations of similar nature are needed for a large number of objects to put some of the possibilities listed above on a more firm foundation since these intuitive ideas based on heuristic modeling have important implications in topics like theory of PDRs, role of dust grains in the galactic chemical history and evolution.

Appendix A: Some strong UV lines predicted

Label	line	Model Flux $H\beta = 100$
Fe 2	1216A	49.4
He 2	1640A	384.9
He 2	1215A	121.8
He 2	1085A	55.5
He 2	1025A	30.5
He 2	3203A	23.1
C 3	1910A	132.4
C 3	1907A	137.3
C 4	1551A	164.8
C 4	1548A	341.5
N 3	1752A	30.9
N 3	1751A	49.7
N 3	991.0A	29.6
N 4	1486A	130.9
N 4	1485A	166.4
N 5	1243A	82.4
N 5	1239A	174.0
TOTL	1665A	23.8
TOTL	1402A	30.1
O 5	1218A	27.7
O 5	1211A	37.1
TOTL	1035A	25.7
Ne 4	2424A	66.3
TOTL	2798A	33.2
Mg 2	2796A	22.1

References

Abel, N. P., Ferland, G. J., Shaw, G., & van Hoof, P. A. M. 2005, ApJS, 161, 65
Acker, A., Koppen, J., Stenholm, B. R., et al. 1991, A&AS, 89, 237
Acker, A., Ochsenbein, F., Stenholm, B., et al. 1992, Strasb.-ESO Catalogue
Aller, L. H., & Keyes, C. D. 1987, ApJS, 65, 405
Asplund, M., Grevesse, N., & Sauval, A. J. 2005, ASPC, 336, 25
Benjamin, R. A., Skillman, E. D., & Smits, D. P. 1999, ApJ, 514, 307
Bernard Salas, J., Pottasch, S. R., Beintema, D. A., & Wesselius, P. R. 2001, A&A, 367, 949
Cahn, J. H., Kaler, J. B., & Stanghellini, L. 1992, A&AS, 94, 399
Condon, J. J., & Kaplan, D. L. 1998, ApJS, 117, 361
Corradi, R. L. M., & Schwartz, H. E., A&A, 269, 462
Davis, C. J., Smith, M. D., Luke Stern, et al. 2003, MNRAS, 344, 262
Draine, B. T., & Bertoldi, F. 2000, in H_2 in Space (Cambridge Univ. Press), 131
Exter, K. M., Barlow, M. J., & Walton, N. A. 2004, MNRAS, 349, 1291
Feldman, U., & Widing, K. G. 2003, Sp. Sci. Rev., 107, 665
Ferland, G. J., Korista, K. T., Verner, D. A., et al. 1998, PASP, 110, 761
Fluks, M. A., Plez, B., de Winter, D., et al. 1994, A&AS, 105, 311
Habart, E., Walmsley, M., Verstraete, L., et al. 2005, Sp. Sci. Rev., 119, 71
Hollenbach, D. J., & Tielens, A. G. G. M. 1997, ARA&A, 35, 179
Hora, J. L., Latter, W. B., & Deutsch, L. K. 1999, ApJS, 124, 195
Hummer, D. G., & Storey, P. J. 1987, MNRAS, 224, 801
Karakas, A. I. 2003, Thesis, Monash Univ. Melbourne
Kerber, F., Mignani, R. P., Guglielmetti, F., et al. 2003, A&A, 408, 1029
Klaas, U., Walker, H. J., Müller, T. G., et al. 2006, A&A, 452, 523
Milne, D. K., Aller, L. H. 1982, A&AS, 50, 209
Odell, C. R. 1963, ApJ, 138, 1963
Peeters, E., Hony, S., van Kerckhoven, C., et al. 2002, A&A, 390, 1089
Phillips, J. P., & Mampaso, A. 1988, A&A, 190, 237
Phillips, J. P., & Mampaso, A. 1989, A&A, 218, 257
Phillips, J. P., Williams, P. G., Mampaso, A., & Ukita, N. 1992, AP&SS, 188, 171
Pishmish, P., Manteiga, M., & Recio, A. M. 2000, in ASP Conf. Ser. 199 (San Francisco), ed. J. H. Kastner, et al., 397
Pottasch, S. R., & Acker, A. 1989, A&A, 221, 123
Pottasch, S. R., & Beintema, D.A. 1999, A&A, 347, 974
Pottasch, S. R., & Bernard-Salas, J. 2006, A&A, 457, 189
Pottasch, S. R., Wesselius, P. R., Wu, C. C., et al. 1977, A&A, 54, 435
Pottasch, S. R., Preite-Martinez, A., Olnon, F. M., et al. 1986, A&A, 161, 363
Pottasch, S.R., Beintema, D. A., & Feibelman, W. A. 2000, A&A, 363, 767
Pottasch, S. R., Beintema, D. A., Bernard-Salas, J., & Feibelman, W. A. 2001, A&A, 380, 684
Pottasch, S. R., Beintema, D. A., Bernard Salas, J., et al. 2002, A&A, 393, 285
Preite-Martinez, A., & Pottasch, S. R. 1983 A&A, 126, 31
Rauch, T. 2003, A&A, 403, 709
Shaw, G., Ferland, G. J., Abel, N. P., et al., 2005, ApJ, 624, 794
Sternberg, A., & Dalgarno, A. 1989, ApJ, 338, 197
Surendiranath, R., Pottasch, S. R., & García-Lario, P. 2004, A&A, 421, 1051
Tielens, A. G. G. M., & Hollenbach, D. 1985, ApJ, 291, 722
Tylenda, R., Siodmiak, N., Gorny, S. K., et al., 2003, A&A, 405, 627
van Hoof, P. A. M., Weingartner, J. C., Martin, P. G., et al. 2004, MNRAS, 350, 1330
Wang, W., Liu, X.-W., Zhang, Y., & Barlow, M. J. 2004, A&A, 427, 873
Weingartner, J. C., & Draine, B. T. 2001, ApJS, 134, 263
Zeippen, C. J. 1982, MNRAS, 198, 111
Zeippen, C. J. 1987, A&A, 173, 410